Published 5/17/16 as Kyle M. McElhinny, Gokul Gopalakrishnan, Donald E. Savage, David A. Czaplewski, Max G. Lagally, Martin V. Holt and Paul G. Evans, "Synchrotron x-ray thermal diffuse scattering probes for phonons in Si/SiGe/Si trilayer nanomembranes," MRS Advances doi:10.1557/adv.2016.352 (2016). http://journals.cambridge.org/abstract_S2059852116003522

Synchrotron x-ray thermal diffuse scattering probes for phonons in Si/SiGe/Si trilayer nanomembranes

Kyle M. McElhinny[1], Gokul Gopalakrishnan[1†], Donald E. Savage[1], David A. Czaplewski[2], Max G. Lagally[1], Martin V. Holt[2], Paul G. Evans[1*]

[1] Materials Science and Engineering, University of Wisconsin-Madison, Madison, WI 53706, USA

[2] Center for Nanoscale Materials, Argonne National Laboratory, Argonne, IL 60439, USA

*** Corresponding author. E-mail: pgevans@wisc.edu**

†Present address: Engineering Physics, University of Wisconsin-Platteville, Platteville, WI 53818, USA

ABSTRACT

Nanostructures offer the opportunity to control the vibrational properties of via the scattering of phonons due to boundaries and mass disorder as well as through changes in the phonon dispersion due to spatial confinement. Advances in understanding these effects have the potential to lead to thermoelectrics with an improved figure of merit by lowering the thermal conductivity and to provide insight into electron-phonon scattering rates in nanoelectronics. Characterizing the phonon population in nanomaterials has been challenging because of their small volume and because optical techniques probe only a small fraction of reciprocal space. Recent developments in x-ray scattering now allow the phonon population to be evaluated across all of reciprocal space in samples with volumes as small as several cubic micrometers. We apply this approach, synchrotron x-ray thermal diffuse scattering (TDS), to probe the population of phonons within a Si/SiGe/Si trilayer nanomembrane. The distributions of scattered intensity from Si/SiGe/Si trilayer nanomembranes and Si nanomembranes with uniform composition are qualitatively similar, with features arising from the elastic anisotropy of the diamond structure. The TDS signal for the Si/SiGe/Si nanomembrane, however, has higher intensity than the Si membrane of the same total thickness by approximately 3.75%. Possible origins of the enhancement in scattering from SiGe in comparison with Si include the larger atomic scattering factor of Ge atoms within the SiGe layer or reduced phonon frequencies due to alloying.

INTRODUCTION

In nanomaterials, the periodic mechanical boundary conditions found in bulk systems are replaced by conditions representing free surfaces separated by a small number of crystalline unit cells [1–3]. This mechanical difference has a vast impact on the vibrational properties, leading to the introduction of low-symmetry vibrational modes that are not found in the bulk. The scaling of vibrational properties with the size of the system leads to the possibility that vibrational properties can be controlled through structural modification and nanopatterning. This phonon engineering has a variety of applications [4]. An additional degree of freedom in the design of Si-based group-IV nanomaterials is obtained by including SiGe alloys in the structure. First, the increased mass of Ge leads to a reduction in phonon frequencies. Lattice dynamics calculations for an $Si_{1-x}Ge_x$ alloy with x=12.5% predict, for example, that phonon energies are reduced by 0.4 meV at the boundary of the Brillouin zone, in comparison with Si [5]. In addition, the randomness of Ge substitution into the diamond structure leads to mass-disorder scattering and causes SiGe to have different vibrational properties that pure Si or Ge [6].

With the free-surface boundary conditions of nanomaterials, elastic continuum theory predicts new dilatational, flexural, and shear modes [1,2,7]. Dilatational and flexural modes can be thought of as being symmetric or asymmetric, respectively, when inverted through a fixed point in the center of the membrane. Both of these modes have a combination of the longitudinal and transverse polarization of the atomic displacements that would be used to characterize bulk modes. The shear modes have only transverse character [1,7]. Spatial confinement results in the shifting of phonon modes away from well-defined bands to a much larger number of phonon frequencies than are observed in bulk systems [1,2]. The creation of these new modes affords the opportunity to modify the phonon modes responsible for carrying thermal energy because some of these new modes have energies lower than bulk modes with the same wavevector. The modes with lower frequency extend across the Brillouin zone, posing a characterization challenge because optical techniques such as Raman and Brillouin scattering probe only a small range of wavevectors near the center of the Brillouin zone.

X-ray thermal diffuse scattering allows phonon populations to be probed across the entire range of relevant wavevectors, spanning the full extent of the three-dimensional Brillouin zone. Here we use this approach to compare the phonon populations Si/SiGe/Si trilayer nanomembranes to the populations in Si nanomembranes. Obtaining high-wavevector insight into the phonon dispersion and populations is particularly important in understanding thermal conductivity in Si and SiGe. In both of these materials, significant contributions to thermal conductivity arise from phonons with energies above approximately 1 meV, particularly at elevated temperatures relevant to thermoelectric applications [6]. Acoustic phonons with energies in this range are far from the zone center, with wavevectors on the order of 10% or more of the zone boundary momentum, making a large-wavevector probe particularly important.

Thermal diffuse scattering arises from the fluctuations of atomic positions resulting from the thermal population of vibrational modes. The displacement of the atoms from their lattice sites results in a reduction of the intensities of Bragg reflections by the Debye Waller factor [8]. The intensity lost from the Bragg reflections is redistributed across reciprocal space as thermal diffuse scattering (TDS). The distribution of TDS intensity is directly related to the phonon population. In the first-order approximation of the TDS signal, the intensity at total scattering wavevector $\boldsymbol{S}$ is related to the phonon population within the Brillouin zone at wavevector $\boldsymbol{Q}=\boldsymbol{S}-\boldsymbol{G}$, where $\boldsymbol{G}$ is the reciprocal lattice point closest to $\boldsymbol{S}$ [8]. The momentum of x-ray photons is sufficiently large that phonons across the entire Brillouin zone can be probed via TDS. TDS simulations of thermal diffuse scattering can very accurately reproduce the scattering observed from bulk crystals, and by comparing the simulations with experimental results, the distribution of TDS intensity can be used to determine key parameters of the phonon dispersion [9].

EXPERIMENT

The structure of the Si/SiGe/Si trilayer and of uniform-composition Si nanomembranes considered in this study are shown in Fig. 1. The details of the processing steps involved in membrane fabrication processes are given in refs. [10] and [11]. The design of both types of membranes incorporates features aimed at minimizing the distortion due to bending arising from residual stress. The Si/SiGe/Si nanomembrane, shown in Fig. 1(a), has a total thickness of 60 nm. The SiGe layer has a composition of $Si_{0.76}Ge_{0.24}$, and each Si and SiGe layer has equal 20 nm thicknesses in order to minimize bending stresses. The biaxial expansion upon releasing the Si/SiGe/Si structure results in buckling that is removed by forming a strain-relief pattern consisting of narrow arms connecting a flat nanomembrane with width of 100 μm to the substrate [11]. The layer structure and arm structure of the Si/SiGe/Si structure are shown in Fig.

1(a). The Si nanomembranes were formed using a similar series of steps resulting in the formation of a window with a width of 200 μm, as shown in Fig. 1(b) [10]. The excess length associated with the residual stress in the Si nanomembrane, corresponding to a strain of 0.1%, was accommodated by using the thickness step of the 400-nm-thick buried SiO_2. This edge-induced flattening processing step depends on interfacial energies during the drying the Si nanomembranes after etching to release the nanomembrane from the buried oxide layer [10]. Optical profilometry images illustrating the flatness of Si/SiGe/Si and Si nanomembranes with thickness of 60 nm, 97 nm, and 21 nm are shown in Figs. 1 (c), (d) and (e), respectively. The Si/SiGe/Si structure was fabricated through the thermal oxidation of the SOI device layer to a thickness of 20 nm followed by subsequent growth of the SiGe and top Si layer by chemical vapor deposition.

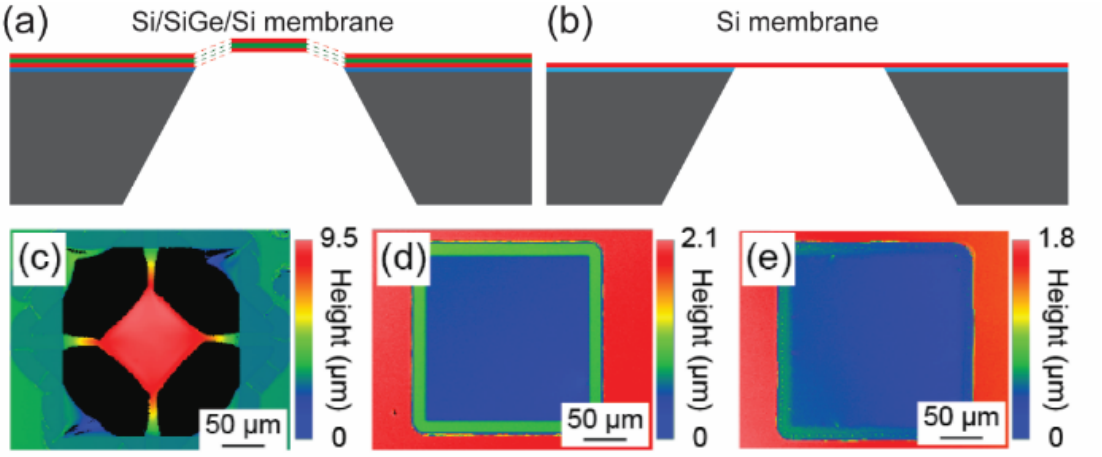

Figure 1. Schematics of (a) Si/SiGe/Si trilayer nanomembrane and (b) Si nanomembrane. Optical profilometry images of (c) the Si/SiGe/Si trilayer connected to the substrate by narrow arms, and Si nanomembranes with thicknesses of (d) 97 nm and (e) 21 nm.

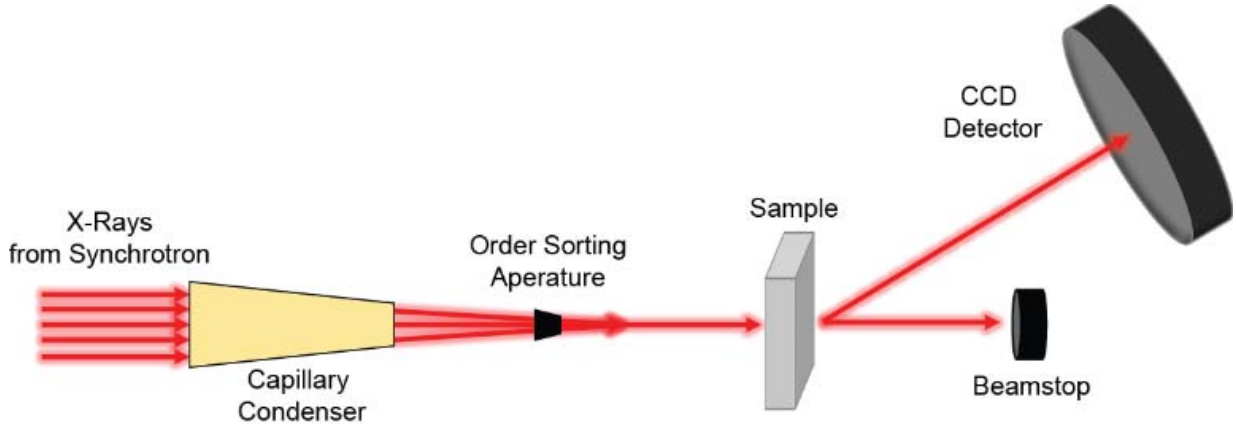

Figure 2. Synchrotron x-ray thermal diffuse scattering studies of nanomembranes. The x-ray optics, nanomembrane sample, and beam stop were in vacuum to reduce the scattered background intensity. X-rays exited the vacuum chamber through a Be window and were collected by a CCD x-ray detector.

X-ray scattering experiments were carried out at station 26-ID-C of the Advanced Photon Source at Argonne National Laboratory using the arrangement shown in Fig. 2. A 10 keV x-ray beam was focused by a capillary condenser to a 30 μm spot at the sample. The total flux of x-

rays in the focused beam was approximately 10^{12} photons/sec. The x-ray optics and sample were mounted in vacuum in order to eliminate contributions to the diffuse scattering signal arising from air scattering. The x-ray beam passed through the membranes in a transmission geometry and a Pb beam stop was employed to absorb the transmitted beam beyond the sample. The TDS intensity distribution was recorded using a charge-coupled device (CCD) x-ray detector (Mar Inc.) with a pixel size of 80 μm and a diameter of 165 mm. The detector provided an image across a cone with an opening angle of 15°. The center of the detector was located at an angle of 31.94° above the horizontal scattering plane, at a horizontal scattering angle of 35.85°. A series of Pb foil shields, tapering from the Be exit window to the sample, were employed to reduce non-sample scattering sources. Exposure times of 600 s were used to collect sufficient TDS statistics. The images were double correlated to eliminate artifacts arising from cosmic radiation.

RESULTS

The experimentally measured distributions of x-ray thermal diffuse scattering intensities for three nanomembrane samples are shown in Fig. 3. The scattering patterns were collected from the trilayer Si/SiGe/Si nanomembrane with a total thickness of 60 nm, and Si membranes with thicknesses of 21 nm and 97 nm, respectively. These scattering patterns are two-dimensional slices of the three-dimensional reciprocal space of the nanomembranes. The intersection of the two-dimensional scattering pattern with the three-dimensional boundaries of Brillouin zones centered at the diamond cubic reciprocal lattice points are drawn as orange lines superimposed on the scattering patterns in Fig. 3. The zone with the largest area at the tops of the images in Fig. 3 is centered on the -3 -1 1 reciprocal lattice point.

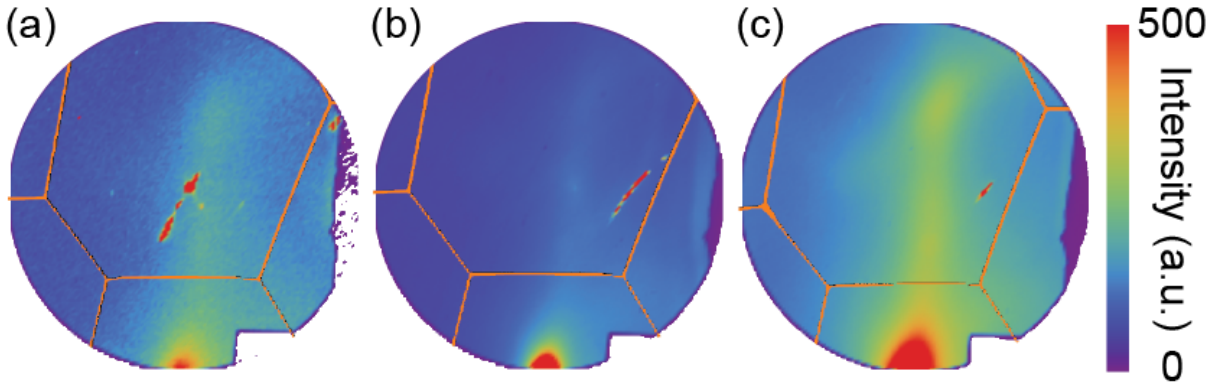

Figure 3. X-ray thermal diffuse scattering patterns acquired from (a) a 60 nm-thick, Si/SiGe/Si trilayer nanomembrane, (b) a 21 nm-thick Si nanomembrane, and (c) a 97 nm-thick Si nanomembrane. Orange lines are overlaid on the detector image to indicate the intersection of the Ewald sphere with the Brillouin zone boundaries.

Each scattering pattern in Fig. 3 exhibits a broad distribution across the entire detector as well as streaks of locally higher TDS intensity. These streaks of intensity extend approximately vertically in the image as well as along a line from the center to the upper right corner. The loci of wavevectors along these streaks correspond to directions in reciprocal space close to the high symmetry directions, [111] and [100], respectively, of Si and Ge. Phonon modes along these directions have lower frequency and hence exhibit a larger TDS intensity. Two additional sets of features are also apparent in Fig. 3. An intense region at the bottom of the detector arises from the high population of low-frequency modes near the Brillouin zone center. Sharp highly localized high-intensity artifacts in the scattering pattern arise from diffraction from optical elements that was not completely obscured by the Pb shielding.

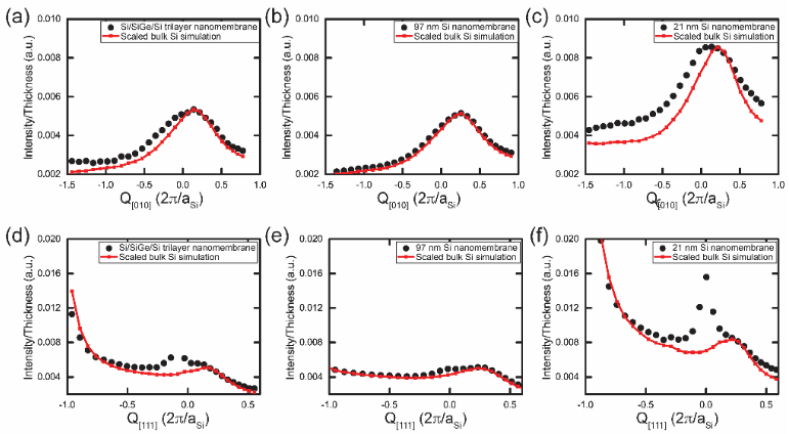

Figure 4. TDS intensity profiles extracted along the intense streaks of intensity observed in Fig. 3. (a), (b), and (c) Observed (points) and simulated (red line) intensity profiles approximately along [010]. (d), (e), and (f) Observed (points) and simulated (red line) intensity profiles approximately along [111]. Sharp features in (d) and (f) and the weaker feature in (e) at $Q_{[111]} \approx 0$ correspond to the intensity from the crystal truncation rod of the membrane and do not arise from TDS.

The observed intensities can be systematically compared with the TDS scattering pattern expected for bulk Si by plotting the simulated and observed intensities along specific directions of the TDS data. Figures 4(a)-(c) show the observed and simulated intensity along a direction of the images in Fig. 3 that lies approximately along [010]. Each profile is normalized by the thickness to illustrate any regions of unexpectedly high intensity. Figures 4(d)-(f) show profiles extracted along [111] directions. For each sample the simulated intensity is scaled by a single overall parameter to fit both profiles. The 21 nm Si nanomembrane exhibits excess intensity along both crystallographic directions, consistent with our previous study [12]. The Si/SiGe/Si trilayer yields an intensity distribution that is qualitatively similar to the Si simulation.

DISCUSSION

There is excellent agreement between the observed and simulated intensity for the thickest, 97 nm, Si nanomembrane. As is apparent in Fig. 3, the thinner Si nanomembrane and the Si/SiGe/Si trilayer nanomembrane exhibit qualitatively similar distributions of scattered intensity. A comparison with the 21 nm nanomembrane intensity with the simulation shows that the experimentally observed intensity follows approximately the expected distribution in reciprocal space, but with a higher-than-expected intensity. We have previously discussed the possibility that this excess can arise from the modification of phonon frequencies due to the free surface mechanical boundaries [12]. The mechanical discontinuities in the Si/SiGe/Si system are not sufficiently large to introduce spatial confinement of the phonon modes and consequently the intensity of the scattering is quantitatively very similar to what would be expected from a bulk Si membrane of the same thickness. There is, however, an excess of intensity of 3.75% along [010] in the Si/SiGe/Si trilayer membrane and a broadening of the TDS profile, pointing to vibrational differences between Si/SiGe/Si and the thicker Si membrane. Possible origins of the enhancement in scattering from SiGe in comparison with Si include the larger atomic scattering factor of Ge atoms with the SiGe layer or reduced phonon frequencies due to alloying.

CONCLUSIONS

The rapidly evolving experimental capability to create low-dimensional materials for electronic and thermal applications poses a significant characterization challenge. X-ray TDS

measurements allow the phonon population in nanoscale materials to be probed across the entire range of relevant wavevectors and exposes systematic trends in phonon population as a function of thickness and composition. Future time-resolved diffuse scattering experiments offer a possible extension of this technique, providing additional insight into both the effects of alloying and spatial confinement on phonon lifetimes as well as populations [13,14].

ACKNOWLEDGMENTS

GG, KM, and PE acknowledge support from the US AFOSR, through contract FA9550-10-1-0249 for the development of diffuse scattering methods and from the U.S. DOE, Basic Energy Sciences, Materials Sciences and Engineering, under contract no. DE-FG02-04ER46147 for the development of x-ray scattering analysis techniques. Nanomembranes were fabricated at the Wisconsin Center for Applied Microelectronics at UW-Madison, supported in part by the UW MRSEC (NSF DMR-1121288), and at the Center for Nanoscale Materials at Argonne National Laboratory. The Center for Nanoscale Materials, an Office of Science user facility, is supported by the U. S. Department of Energy, Office of Science, Office of Basic Energy Sciences, under Contract No. DE-AC02-06CH11357. Use of the Advanced Photon Source was supported by the U. S. Department of Energy, Office of Science, Office of Basic Energy Sciences, under Contract No. DE-AC02-06CH11357. Development and maintenance of the growth facilities used for fabricating samples is supported by the U.S. DOE (DE-FG02-03ER46028). KM acknowledges support from 3M Corporation through 3M Science and Technology Fellowship Program.

REFERENCES

[1] N. Bannov, V. Mitin, and M. Stroscio, Phys. Status Solidi B **183**, 131 (1994).
[2] J. Cuffe, E. Chávez, A. Shchepetov, P.-O. Chapuis, E. H. El Boudouti, F. Alzina, T. Kehoe, J. Gomis-Bresco, D. Dudek, Y. Pennec, B. Djafari-Rouhani, M. Prunnila, J. Ahopelto, and C. M. Sotomayor Torres, Nano Lett. **12**, 3569 (2012).
[3] A. Balandin and K. L. Wang, Phys. Rev. B **58**, 1544 (1998).
[4] A. A. Balandin, J. Nanosci. Nanotechnol. **5**, 1015 (2005).
[5] T. Hori, T. Shiga, and J. Shiomi, J. Appl. Phys. **113**, 203514 (2013).
[6] J. Garg, N. Bonini, B. Kozinsky, and N. Marzari, Phys. Rev. Lett. **106**, 045901 (2011).
[7] H. Lamb, Proc. R. Soc. Lond. Ser. A **93**, 114 (1917).
[8] J. Als-Nielsen and D. McMorrow, *Elements of Modern X-Ray Physics*, 2nd ed (Wiley, Hoboken, 2011).
[9] M. Holt, Z. Wu, H. Hong, P. Zschack, P. Jemian, J. Tischler, H. Chen, and T.-C. Chiang, Phys. Rev. Lett. **83**, 3317 (1999).
[10] G. Gopalakrishnan, D. A. Czaplewski, K. M. McElhinny, M. V. Holt, J. C. Silva-Martínez, and P. G. Evans, Appl. Phys. Lett. **102**, 033113 (2013).
[11] K. M. McElhinny, G. Gopalakrishnan, D. E. Savage, J. C. Silva-Martínez, M. G. Lagally, M. V. Holt, and P. G. Evans, J. Phys. Appl. Phys. **48**, 015306 (2015).
[12] G. Gopalakrishnan, M. V. Holt, K. M. McElhinny, J. W. Spalenka, D. A. Czaplewski, T. U. Schülli, and P. G. Evans, Phys. Rev. Lett. **110**, 205503 (2013).
[13] M. Trigo, J. Chen, V. H. Vishwanath, Y. M. Sheu, T. Graber, R. Henning, and D. A. Reis, Phys. Rev. B **82**, 235205 (2010).
[14] M. Trigo, M. Fuchs, J. Chen, M. P. Jiang, M. Cammarata, S. Fahy, D. M. Fritz, K. Gaffney, S. Ghimire, A. Higginbotham, S. L. Johnson, M. E. Kozina, J. Larsson, H. Lemke, A. M. Lindenberg, G. Ndabashimiye, F. Quirin, K. Sokolowski-Tinten, C. Uher, G. Wang, J. S. Wark, D. Zhu, and D. A. Reis, Nat. Phys. **9**, 790 (2013).